XRD phase investigations of steam oxidized Fe and Ni rich Cr alloys

Tomasz Dudziak[1], Małgorzata Witkowska[2], Wiktoria Ratuszek[2], Krzysztof Chruściel[2]

[1]Foundry Research Institute, ul. Zakopiańska 73, 30-418 Krakow, Poland
[2]AGH University Science and Technology, Faculty of Metals Engineering and Industrial Computer Science,
al. A. Mickiewicza 30, 30-059 Krakow, Poland

E-mail: tomasz.dudziak@iod.krakow.pl

Abstract

The aim of this work was to summarise XRD investigations performed after the tests carried out in steam oxidation conditions in the temperature range 700−800°C for 3000 hours. In this work, two solid-solution strengthened alloys; Haynes® 230®, 617 alloy and two (γ') gamma-prime strengthened alloys; 263 and Haynes® 282® and high alloyed steels rich in Cr: 309S, 310S and HR3C were exposed. The phase analyses were carried out using two techniques; Bragg-Brentano (BB) geometry and geometry of constant angle called grazing incidence $\alpha = 1°$ and $\alpha = 3°$.

Keywords: austenitic steel, Ni based alloys, high temperature, steam, XRD

1. Introduction

Coal fired power generation is one of the key industrial technologies in energy production worldwide. However, energy produced from coal creates a large quantity of CO_2 emission, while this technology used in many plants is rather old and inefficient. These old technologies in coal fired power plants based on sub-critical conditions (SbC) required low pressure and low temperatures [1]. The steam pressure and temperature are adequate to the steel material used in the operation, i.e. low grade steels like T/P22 (2.5 wt. % Cr), T/P91 (9 wt. % Cr) are used with limited functionality and temperature below 600°C. Their applicability (performance) is limited due to the formation of thick, non-protective oxide scales consisting of predominantly iron oxides. Furthermore, due to large emission of CO_2 from sub-critical conditions of power plants, the European Union introduced recent legislations, which demand the reduction of

CO_2 to about 20−30% by 2020. Nevertheless, electric power generation from coal firing technology still can be maintained but through a more secure and sustainable route, using a new generation of coal power plants with operating temperatures above 700°C or even more in regions of super heaters and re-heaters. According to the High Efficiency Low Emission roadmap for coal technology, prepared by International Energy Agency in 2012, these old and inefficient coal fired processes for sub-critical conditions should be replaced by more advanced technologies utilizing new units with higher efficiency for Ultra-Supercritical Conditions (USC) and Advanced-Ultra-Supercritical Conditions (A-USC) steam parameters [2]. It requires the use of these processes at not only high temperatures but also utilizing higher purity oxidation conditions. Steel materials with Cr contents of 2−10% cannot withstand these USC and A-USC service conditions due to their quick oxidation rates and destruction. Currently, particular attention is focused on the austenitic steels with high Cr content (>20 wt. %), such as 309S 310S or HR3C stainless steel or more technologically advanced Ni based alloys, where adequate mechanical properties are combined with high temperature corrosion resistance owing to the formation of continuous, thin, adherent, thermally grown oxide Cr_2O_3 scale [3,4,5].

Nevertheless, under long term exposure even 310S and other Cr-rich and Ni-rich steels and alloys undergo degradation due to breakaway oxidation [6,7,8,9]. Therefore, it is important to investigate phase changes under different temperature conditions to evaluate corrosion at high temperature processes. Development during exposure, particular phases in Cr rich materials, like: Fe_2O_3, Fe_3O_4 in austenitic steels or NiO, compound in Ni based Cr rich alloys to a large extent may suggest the development of non-protective oxide scale that may

initiate and lead to breakaway oxidation. Therefore, it is important to investigate phase changes under different temperature conditions in order to evaluate corrosion degradation at the high temperature process for longer exposure times. Hence, in this work an effort is placed to investigate the phase formation under steam oxidation conditions in order to examine corrosion processes. The steam oxidation tests were carried out in the temperature range 700−800°C for 3000 hours. In this work, two solid-solution strengthened alloys; Haynes® 230®, 617 alloy and two (γ') gamma-prime strengthened alloys; 263 and Haynes® 282® together with high alloyed steels: 309S, 310S and HR3C were exposed. The phase analyses were carried out using Bragg-Brentano (BB) geometry and geometry of constant angle that is called grazing incidence α = 1° and α = 3°.

2. Experimental procedure

2.1. Materials

In the study, seven alloys were exposed; two solid-solution strengthened alloys; Haynes® 230®, 617 alloy and two gamma-prime (γ') strengthened materials; 263 alloy and Haynes® 282® and high alloyed steels rich in Cr: 309S, 310S and HR3C. Table 1 shows nominal compositions according to producer certificates of the high-alloyed steels and Ni based alloys respectively.

Prior to steam process at 700−800°C, the materials were cut out from the plates in small squares (20 mm^2). As mentioned, HR3C alloy was delivered as a tube section, the material was machined into tube segments, which had dimensions of a ~15 mm length, × 10 mm width chord, with a 4 mm wall thickness. The surface of the steels and Ni based alloys was ground using 600 grit SiC paper. Furthermore, the samples were cleaned in acetone at 40°C for 15 minutes using an ultrasonic bath. Prior to and during the exposure, the samples were accurately weighed using a digital balance with a resolution of ±0.01 mg for masses $m < 80$ g. The digital balance (Sartorius CPA225D) was calibrated frequently using its internal calibration function and periodically with test weights. The oxidised samples in the

first instance were characterised to investigate phase formation using a D500 Kristalloflex from Siemens with monochromatic X-ray sources Cu (αKα = 1.54 A) and an X-ray diffractometer (XRD) (EMPYREAN Panalytical) with a Cu X-ray source using an Ni filter.

2.2. Steam oxidation

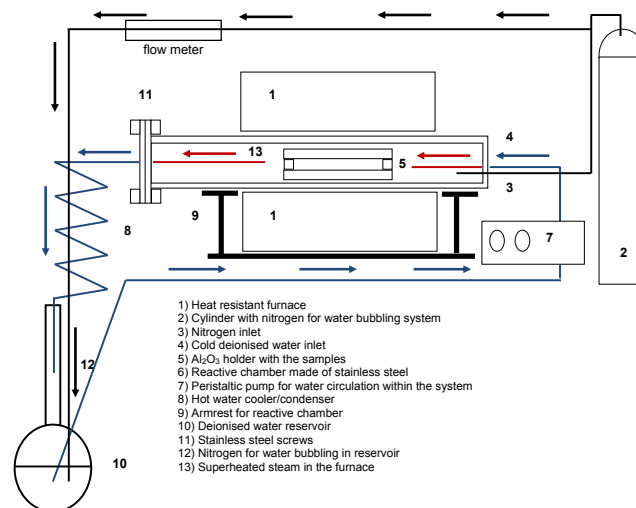The high temperature rig for Ni based and Fe based alloys corrosion assessment is shown in Figure 1.

Fig. 1. Steam oxidation rig used in the experimental procedure

In general, the rig consists of a heat resistant furnace, where a reactive chamber made of 8 mm thick wall 316L stainless steel was used. Inside the reactive chamber an Al$_2$O$_3$ 5 mm thick wall ceramic liner was inserted. The Al$_2$O$_3$ liner prevented steam oxidation reaction with the 316L stainless steel vessel reaction chamber under high temperature exposures. Hence, Al$_2$O$_3$ liner in this work was responsible for constant partial pressure of oxygen during high temperature tests. Deionised water using polyamide cables and 304L stainless steel tubes was delivered by a peristaltic pump with 2.833 ml/min flow rate. Throughout the high temperature tests, deionised water in the reservoir was constantly purged by nitrogen

Table 1. Nominal chemical composition of the materials (wt. %) used in steam oxidation work

	Ni	Fe	Cr	Co	Mo	Si	Mn	Cu	Nb	La	Ti	Al	C	W	B	P	S	N
309S	14	Bal.	23	–	–	0.75	2.0	–	–	–	–	–	0.20	–	–	0.045	0.03	–
310S	21	Bal.	25	–	–	1.50	2.0	–	–	–	–	–	0.08	–	–	0.045	0.03	–
HR3C	20	Bal.	25	–	–	0.75	1.2	–	0.45	–	–	–	0.06	–	–	0.040	0.03	0.2
263 alloy	Bal.	0.6	20	20.0	6.0	0.40	0.6	0.2	–	–	1.2	0.6	0.06	–	–	–	–	–
617 alloy	Bal.	1.0	22	12.5	9.0	–	–	–	–	–	0.3	1.2	0.07	–	–	–	–	–
Haynes® 230®	Bal.	3.0	22	5.0	2.0	0.40	0.5	–	–	0.02	–	0.3	0.10	14	0.015	–	–	–
Haynes® 282®	Bal.	1.5	20	10.0	8.5	0.15	0.3	–	–	–	2.1	1.5	0.06	–	0.050	–	–	–

in order to eliminate oxygen dissolved in water from an ambient atmosphere (air). Nitrogen flow was constantly measured by a flow meter connected to the purging line (50 Nml/min).

The prepared samples were placed on the Al_2O_3 ceramic holder and introduced to the furnace. The furnace was locked using 4 screw made of stainless steel. Further, when the chamber was closed, the nitrogen was run in order to purge the chamber and the samples for 2 hours at 200°C, to remove moisture and other impurities. At the same time, deionised water in the tank was constantly purged. Finally, with the temperature rising to reach the final point, nitrogen flow through the reactive chamber was turned off and peristaltic pump was turned on in order to deliver deionised water to the reactive chamber. As mentioned, the tank with deionised water was purged constantly by nitrogen from a cylinder, when the test was finished, during cooling period; peristaltic pump was turned off to prevent furnace inundation. Finally, the samples were removed from the holder at room temperature (20°C).

2.3. Post experimental procedure

The exposed samples after steam oxidation tests at 700, 750 and 800°C for 3000 hours were investigated using Scanning Electron Microscope (SEM) coupled with Energy-Dispersive X-ray Spectroscopy (EDS) to obtain microstructure observation and chemical composition characterisation. Nevertheless, in this work, the results from XRD investigations are presented only to show changes that are developed under three different temperatures.

2.4. XRD investigations

The phase analyses were performed using two techniques; Bragg-Brentano (BB) geometry and the geometry of constant angle called grazing incidence using $\alpha = 1°$ and $\alpha = 3°$. In Bragg-Brentano (BB) geometry, depth penetration of X-rays can be estimated using the following formula:

$$X = \frac{-\ln(1 - Gx)\sin\theta}{2\mu} \quad (1)$$

where:

Gx donates the intensity of the primary X-ray, giving important information related to irradiation volume,

μ – linear absorption coefficient.

In the grazing angle method, X-rays depth penetration was calculated via the following formula:

$$X = \frac{-\ln(1 - Gx)}{\left\{\mu\left[\dfrac{1}{\sin\alpha} + \dfrac{1}{\sin(2\theta - \alpha)}\right]\right\}} \quad (2)$$

where:

Gx donates the intensity of the primary X-ray, giving important information related to irradiated volume, this value is equivalent to 0.95 (95%),

μ – linear absorption coefficient,

α – incidence angle.

The calculated values of Gx (assumption of Gx = 95%) are shown in Table 2.

Table 2. Depth penetration for the selected samples calculated using two different techniques

Sample/ phase	BB geometry, μm	Grazing incidence α = 1°, μm	Grazing incidence α = 3°, μm
309S	2.58−6.53	0.26	0.75
310S	2.89−7.32	0.29	0.84
HR3C	2.76−6.99	0.28	0.80
alloy 263	3.91−9.91	0.39	1.14
alloy 617	4.33−10.96	0.43	1.26
Haynes® 230®	4.23−10.71	0.42	1.23
Haynes® 282®	4.64−11.76	0.47	1.35

3. Results

This section shows XRD results obtained using two different techniques. Figures 2, 3 and 4 show XRD spectra after 3000 hours tests at 700, 750 and 800°C, respectively.

4. Discussion

The aim of this paper was to evaluate the phases that formed on the surface of the two solid-solution strengthened alloys; Haynes® 230®, 617 alloy, two (γ') gamma-prime strengthened alloys; 263 and Haynes® 282® and high alloyed Cr-rich steels: 309S, 310S and HR3C tested in steam at high temperatures for 3000 hours in the temperature range 700−800°C.

4.1. Ni based alloys

The exposure of the two solid-solution strengthened alloys; Haynes® 230®, 617 alloy, and two (γ') gamma-prime strengthened alloys; 263 and Haynes® 282® in
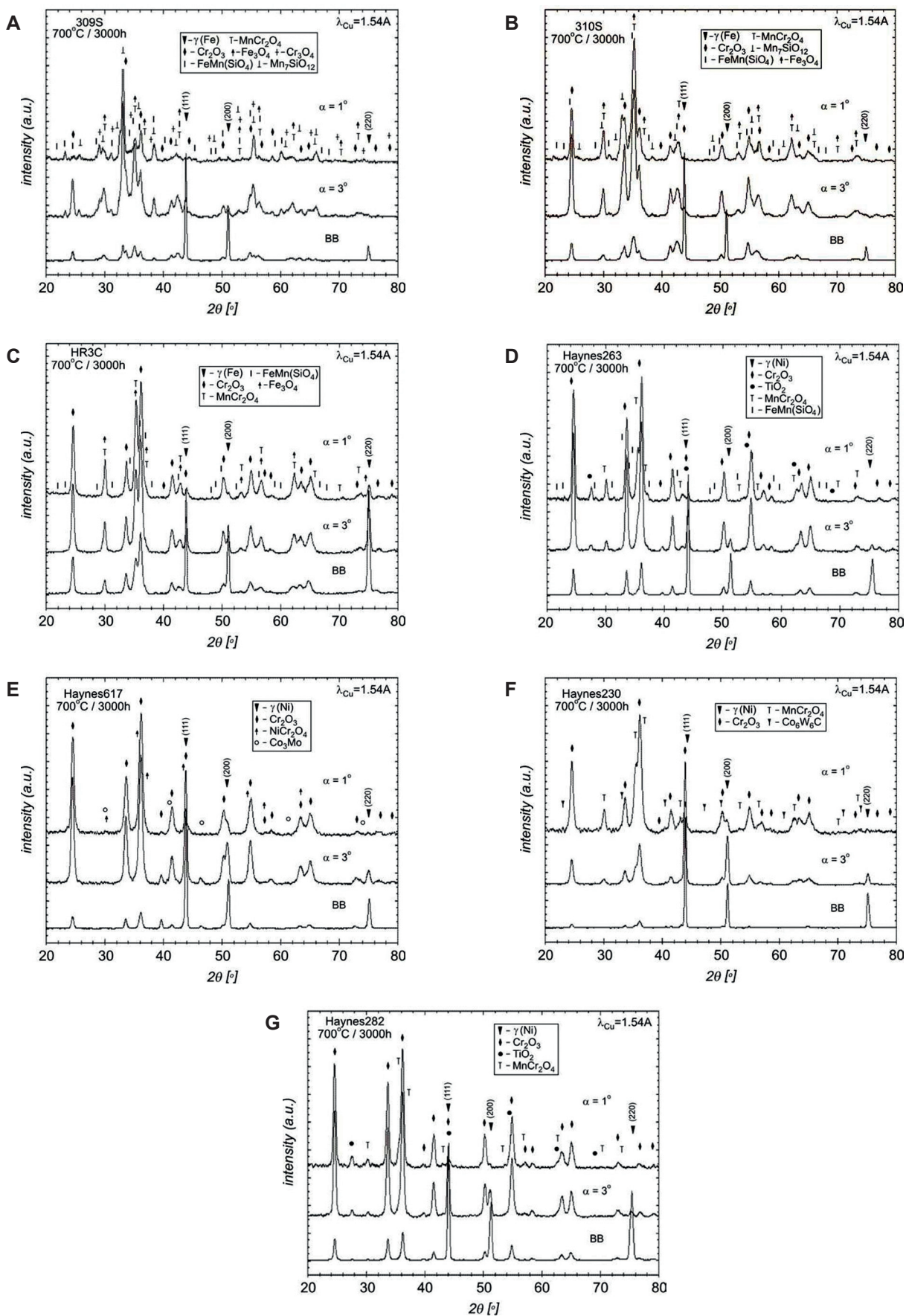
Fig. 2. XRD patterns of advanced austenitic steels and Ni based alloys tested at 700°C for 3000 hours:
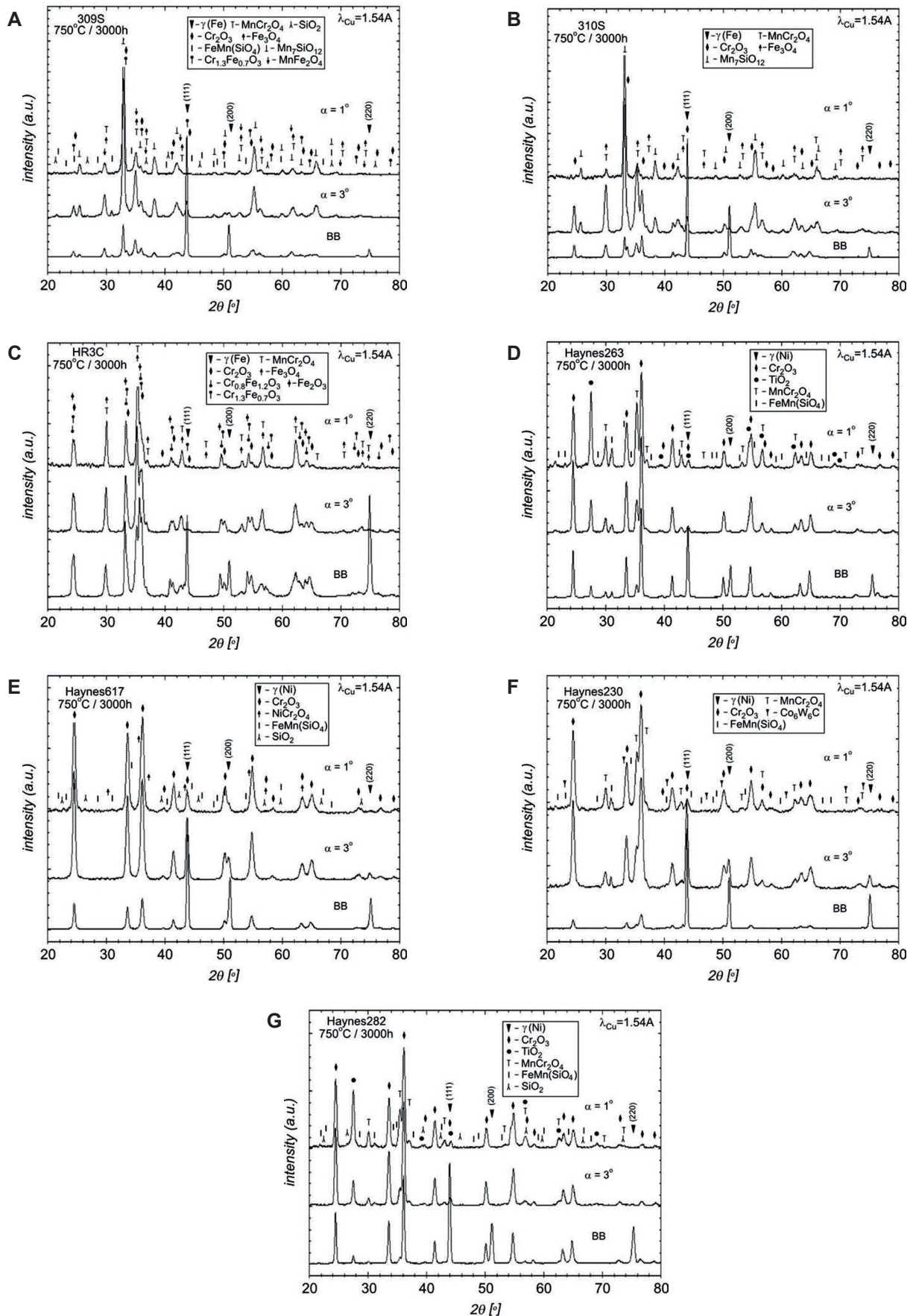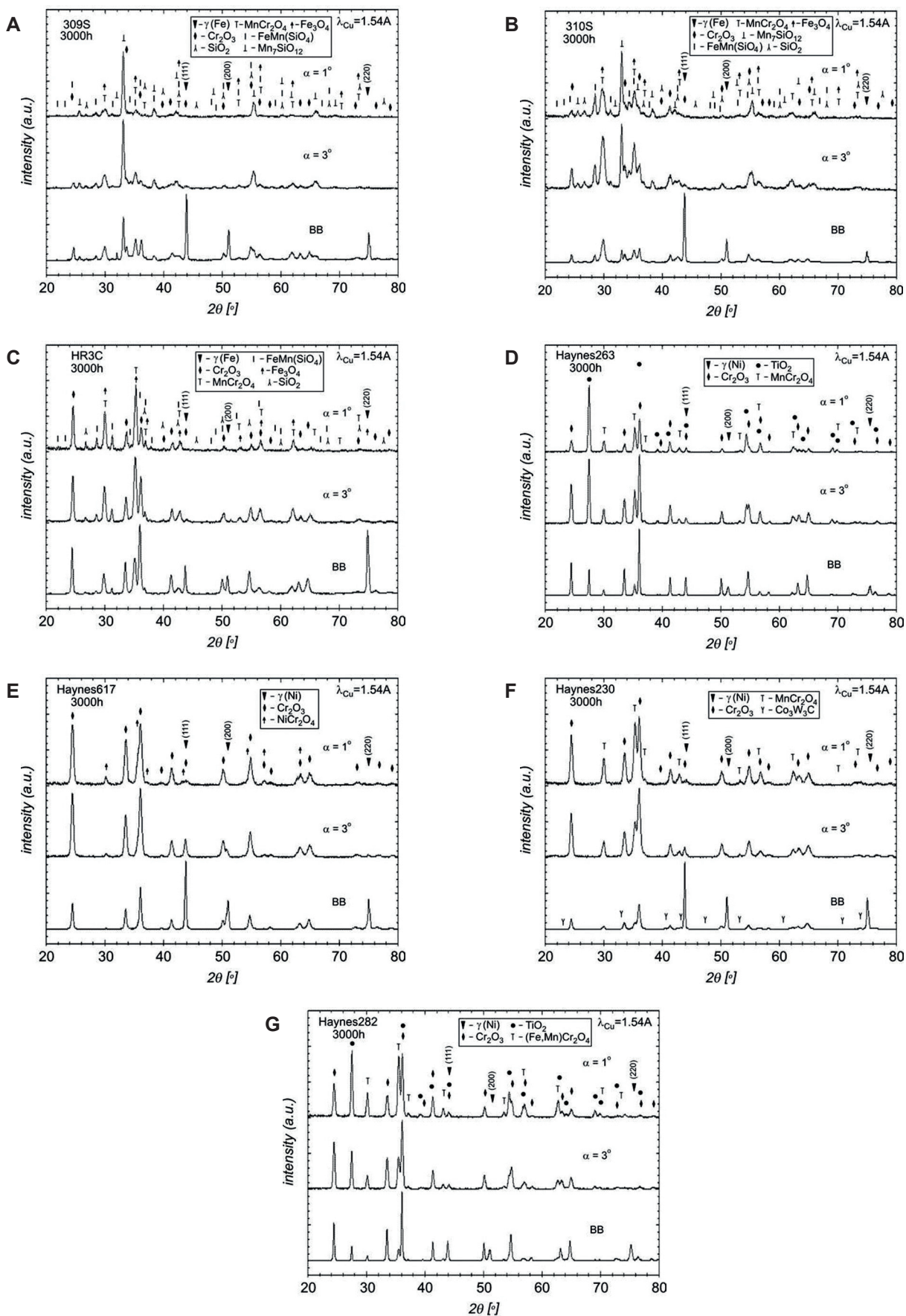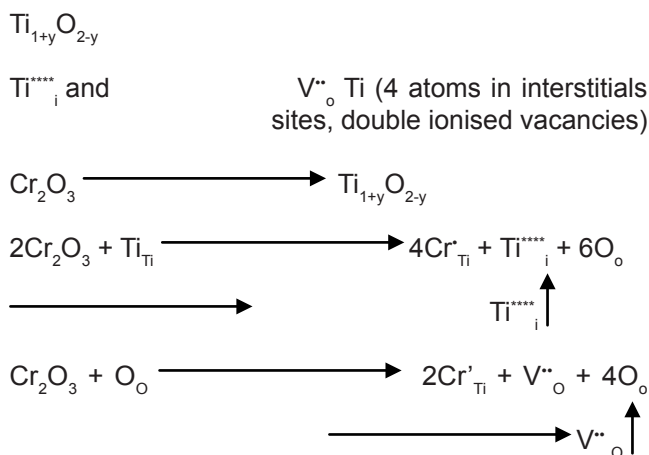A) 309S, B) 310S, C) HR3C, D) alloy 263, E) alloy 617, F) Haynes® 230® and G) Haynes® 282®

Fig. 3. XRD pattern of advanced austenitic steels and Ni based alloys tested at 750°C for 3000 hours: A) 309S, B) 310S, C) HR3C, D) alloy 263, E) alloy 617, F) Haynes® 230® and G) Haynes® 282®

Fig. 4. XRD pattern of advanced austenitic steels and Ni based alloys tested at 800°C for 3000 hours: A) 309S, B) 310S, C) HR3C, D) alloy 263, E) alloy 617, F) Haynes® 230® and G) Haynes® 282®

steam conditions induced development of two main phases: Cr_2O_3 and $MnCr_2O_4$, however, other phases such as: $FeCr_2O_4$ and TiO_2 were also observed. The effect of Mn and Cr is well known in literature. Yang et al. [10] found that additions of higher level of Mn to the Haynes® 230® facilitates the formation of a bi-layered oxide scale: an outer scale consisted of M_3O_4 (M = Mn, Cr, Ni) spinel-rich layer that occupies oxide scale – gas interface over a Cr_2O_3-rich sublayer that is located at the metal – oxide interface. Moreover addition of Mn to Ni based alloys reduces evaporation of Cr from volatile Cr oxyhydroxide at high pressures conditions. Holcomb and Alman [11], suggested that the alloys containing Ti and Mn reduce further the formation of volatile Cr oxyhydroxide from the scale due to the formation of outer layers of TiO_2 or Cr-Mn spinels. Sachitanand et al. [12] reported there is clear evidence of a relationship between high Mn content in the formed oxide scale. When Mn content is high enough, lower Cr volatilisation is observed, nevertheless, higher Mn concentration in the oxide scale shows higher mass gain and the formation of a thicker $MnCr_2O_4$ spinel layer. Holcomb et al. [13] found that Mn additions to Cr rich Ni based alloys decreases the activity of chromium within the oxide, either from solid solution replacement of chromium with manganese (at low levels of manganese) or from the formation of manganese-chromium spinels (at high levels of manganese). This reduction in chromium activity leads to a predicted reduction in chromium evaporation by as much as a factor of 35 at 800°C and 55 at 700°C. Deodeshumkh [14], found as well the beneficial effect of Mn in Haynes® 230® and alloy X, that is one of the most widely used nickel base superalloys for gas turbine engine components. This solid solution strengthened grade possesses a good strength and an excellent oxidation resistance up to 1000°C. The formation of $MnCr_2O_4$ spinel layer is highly beneficial for Ni based alloy, according to work performed by Pedrazzini et al. [15] due to formation of $MnCr_2O_4$ spinel that reduces growth speed of the oxide scale by 1000 times compared with a Mn-free Ni based alloy. It also exhibited improved oxide-metal adhesion, reducing the risk of spallation of the oxide scale.

In general, two solid-solution strengthened alloys showed slightly different phase composition than other two gamma-prime (γ') strengthened alloys. It is assumed that observed changes are due to TiO_2 formation on the surface of the tested alloy. The formation of this phase, in contrast to the $MnCr_2O_4$, is detrimental. It is well known that the TiO_2 phase causes a high number of defects in the crystal structure and is often responsible for accelerated mass gain in TiAl alloys [16,17]. Kekare et al. [18] indicated that the doubly ionised oxygen vacancies are responsible for the kinetic rate of growth of TiO_2 scales on Ti rich alloys and accelerated weight gain leads to reduced oxidation resistance. Cruchley et al. [19] showed that the corrosion degradation of

Ti containing Ni based alloys is greater than that observed in Ti-free samples. The accelerated oxidation rate in Haynes® 282® according to arguments showed by Cruchley et al. [19] is attributed to increased ionic transport caused by doping of the chromia layer by titanium and the creation of vacancies on the chromium sub-lattice, by the reaction presented below:

$$Ti_{1+y}O_{2-y}$$

$$Ti^{****}_i \text{ and} \qquad\qquad V^{\bullet\bullet}_o \text{ Ti (4 atoms in interstitials sites, double ionised vacancies)}$$

$$Cr_2O_3 \longrightarrow Ti_{1+y}O_{2-y}$$

$$2Cr_2O_3 + Ti_{Ti} \longrightarrow 4Cr^{\bullet}_{Ti} + Ti^{****}_i + 6O_o$$

$$\longrightarrow Ti^{****}_i \uparrow$$

$$Cr_2O_3 + O_O \longrightarrow 2Cr'_{Ti} + V^{\bullet\bullet}_O + 4O_o$$

$$\longrightarrow V^{\bullet\bullet}_O \uparrow$$

Doping by Cr atoms leads to the formation of a higher number of defects and enlargement of mass transport throughout point defects.

The effect of Ti addition in Ni based alloys was also reported by Chen et al. [20], Kim et al. [21] and recently by Taylor et al. [22]. Furthermore, they found that Ti has a negative effect on the chromia scale due to the formation of a higher number of chromium vacancies what induces directly higher diffusion rates of the chromium ion through the oxide scale. However, concentration of Ti in the chromia scale is likely to be reduced due to the oxide scale thickening and depletion of Ti in the alloy.

4.2. Austenitic steels

The Cr rich with a small concentration of Si advanced steels, in comparison to the Ni based alloys, have a similar phase structure developed under steam oxidation conditions. The observed corrosion resistance in austenitic steels is attributed to the formation of Cr_2O_3 and $MnCr_2O_3$ rich scale. The role of those oxides in high temperature corrosion was reported previously [4,23]. In contrast to Ni based alloys, Cr rich steels, showed development of Si containing phases: Mn_7SiO_{12}-traces, $(Fe,Mn)SiO_4$ at 700−800°C and SiO_2 at 750 and 800°C that formed as a sublayer between the external oxide scale and the substrate based on cross-sectioned SEM images (not shown here). During XRD investigations after 700°C, no SiO_2 phase was found, perhaps due to the amorphous structure. The formation of amorphous SiO_2 in Si containing austenitic steels as a sublayer in the oxide scale was frequently reported in the past [24,25]. Furthermore, Henry et al. [26], indicated that increasing Si content from 0 to 1 wt. %, in 15 wt. % Cr

austenitic steels enhanced positively steel resistance against breakaway oxidation (delays breakaway oxidation process). The exposed steels, showed a lack of evaporation of Cr from Cr_2O_3 phase due to the formation of $CrO_2(OH)_2$ (g) phase, similar to the Ni based alloys. Lack of the evaporation process in steels and Ni based alloys is firstly due to the formation of $MnCr_2O_4$ phase and secondly due to low O partial pressure that originates from 1 bar steam pressure from the fact that the experiment was carried under 1 bar pressure. Furthermore, the beneficial effect of $MnCr_2O_4$ formation is related not only with reduction or annihilation of the evaporation process but also with reduced formation of Fe_3O_4 phase. In contrast to HR3C steels with 25 wt. % Cr, both steels 309S and 310S with higher Mn addition than that in HR3C underwent a lower degradation rate that is primary related to the Fe rich oxide formation. The formation of such microstructures may indicate initiation of breakaway oxidation in elongated exposures [6]. Ennis et al. [27] reviewed some corrosion works and concluded, that the oxide scales formed on ferritic and austenitic steels change in the following manner (taking into account Cr content): from haematite/magnetite to magnetite/$(Fe,Cr)_3O_4$ spinel to $(Fe,Cr)_3O_4$, spinel/Cr_2O_3 and finally to a pure Cr_2O_3. Thus, the ranking for steam oxidation resistance alloys were proposed (least to most resistant): T23, T91, T92, Super 304H, T347HFG, HR3C, HR6W, HR120, Alloy 230 and Inconel 740. However, the results clearly indicate that even 23−25 wt. % Cr is not sufficient to develop exclusively Cr_2O_3 oxide scale at 700, 750 and 800°C. As mentioned, predominantly Cr_2O_3 and $MnCr_2O_4$ phases form with trace amounts of temperature dependant compounds: $FeMn(SiO_4)$ and SiO_2. Finally, for better traceability of the compound formation, Tables 3−8 show a summary of the phases developed under steam oxidation conditions.

The Tables 3−8 show a summary of the results that were obtained after extensive XRD investigations that were carried out on the exposed Cr rich Fe based alloys and Cr rich Ni based alloys. Based on the achieved results it was found that Cr rich materials show predominantly Cr_2O_3 and $MnCr_2O_4$. The results are in agreement with the results derived from other researchers [1,11,14]. Nevertheless, the obtained results indicate that at 700°C TiO_2 phase is not observed, however the phase appears at 750°C and 800°C where strong peaks are found. Similarly, SiO_2 phase in at 700°C was not observed, at 750°C trace amounts of SiO_2 in 309S steel was found, finally at 800°C, SiO_2 was observed in 309S, 310S and HR3C steel. In addition, the development of less protective phases such as Fe_3O_4 and Fe_2O_3 were observed in Cr rich steels, particularly at 700°C in 309S, 310S and HR3C steel only Fe_3O_4 phase was found.

At 750°C the exposed steels developed both Fe_2O_3 and Fe_3O_4 phases, however Fe_2O_3 as a dominating phase was present in 309S steel. The exposure at 800°C indicated, that the Cr rich steels developed exclusively Fe_3O_4 with no Fe_2O_3 phase. The presence of less protective phases, suggested that Cr rich steels underwent from protective to less protective oxide scale formation, that leads to breakaway oxidation [6,7,28]. Breakaway oxidation is in fact a process where protective properties of the oxide scale are lost due to ambient atmosphere. The rate of breakaway oxidation depends on the microstructure, Cr reservoir in the metal matrix and temperature. Breakaway of stainless steels in different atmospheres and temperatures results in a outward growing Fe rich oxide and an inward growing Fe, Cr (Ni) spinel oxide [5,29]. The spinel microstructure that developed by the inward diffusion process is complex, including both fully oxidized regions and regions of internal oxidation as reported [30].

Table 3. Phase content after 3000 hours steam oxidation at 700°C of austenitic steels: +1 1st, most dominating phase, +2 the 2nd most dominating phase, + presence of a phase, s − trace quantities

Material	Time, h	Geometry	Cr_2O_3	$MnCr_2O_4$	Cr_3O_4	$FeMn(SiO_4)$	Mn_7SiO_{12}	Fe_3O_4
309S	3000	BB	+2	+1	−	+s	+s	+1
		$\alpha = 3°$	+2	+1	−	+	+	+1
		$\alpha = 1°$	+2	+1	−	+	+	+1
310S	3000	BB	+	+2	+s	+	+1	+2
		$\alpha = 3°$	+	+2	+	+	+1	+2
		$\alpha = 1°$	+	+2	+	+	+1	+2
HR3C	3000	BB	+1	+2	−	+s	−	+2
		$\alpha = 3°$	+1	+2	−	+s	−	+2
		$\alpha = 1°$	+1	+2	−	+s	−	+2

Table 4. Phase content after 3000 hours steam oxidation at 700°C of Ni based alloys: +1 1ˢᵗ, most dominating phase, +2 the 2ⁿᵈ most dominating phase, + presence of a phase, s – trace quantities

Material	Time, h	Geometry	Cr_2O_3	$MnCr_2O_4$	$FeCr_2O_4$	TiO_2	$FeMn(SiO_4)$	Co_3Mo	$NiCr_2O_4$	Co_6W_6C
alloy 263	3000	BB	+1	+2	+2	+	+s	–	–	–
		α = 3°	+1	+2	+2	+	+s	–	–	–
		α = 1°	+1	+2	+2	+	+	–	–	–
alloy 617	3000	BB	+1	–	+s	–	–	+2	+s	–
		α = 3°	+1	–	+	–	–	+2	+	–
		α = 1°	+1	–	+	–	–	+s	+	–
Haynes® 230®	3000	BB	+1	+2	+2	–	–	–	–	+
		α = 3°	+1	+2	–	–	–	–	–	+
		α = 1°	+1	+2	–	–	–	–	–	+s
Haynes® 282®	3000	BB	+1	+	+	+2	–	–	–	–
		α = 3°	+1	+	+	+2	–	–	–	–
		α = 1°	+1	+	+	+2	–	–	–	–

Table 5. Phase content after 3000 hours steam oxidation at 750°C of austenitic steels: +1 1ˢᵗ, most dominating phase, +2 the 2ⁿᵈ most dominating phase, + presence of a phase, s – trace quantities

Material	Time, h	Geometry	Cr_2O_3	$MnCr_2O_4$	$FeMn(SiO_4)$	Mn_7SiO_{12}	SiO_2	Fe_3O_4	$Cr_{1.3}Fe_{0.7}O_3$	$MnFe_2O_4$	$Cr_{0.8}Fe_{1.2}O_3$	Fe_2O_3
310S	3000	BB	+1	+	–	+2	–	+	–	–	–	–
		α = 3°	+	+2	–	+1	–	+	–	–	–	–
		α = 1°	+s	+2	–	+1	–	+	–	–	–	–
309S	3000	BB	+	+	+	+1	+	+	+	+2	–	–
		α = 3°	+	+	+	+1	+s	+	+	+2	–	–
		α = 1°	+s	+	+s	+1	+	+	+	+2	–	–
HR3C	3000	BB	+	+2	–	–	–	+	+1	–	+	+1
		α = 3°	+2	+1	–	–	–	+	–	–	+2	–
		α = 1°	+	+1	–	–	–	+	–	–	+2	–

Table 6. Phase content after 3000 hours steam oxidation at 750°C of Ni based alloys: +1 1ˢᵗ, most dominating phase, +2 the 2ⁿᵈ most dominating phase, + presence of a phase, s – trace quantities

Material	Time, h	Geometry	Cr_2O_3	$MnCr_2O_4$	TiO_2	$FeMn(SiO_4)$	$NiCr_2O_4$	Co_6W_6C	SiO_2
alloy 263	3000	BB	+1	+2	+	+	–	–	–
		α = 3°	+1	+	+2	+	–	–	–
		α = 1°	+1	+	+2	+	–	–	–
alloy 617	3000	BB	+1	–	–	+s	–	–	–
		α = 3°	+1	–	–	+s	–	–	–
		α = 1°	+1	–	–	+s	+s	–	+s
Haynes® 230®	3000	BB	+1	+2	–	+s	–	+	–
		α = 3°	+1	+2	–	+	–	+s	–
		α = 1°	+1	+2	–	+	–	–	–
Haynes® 282®	3000	BB	+1	+	+2	+s	–	–	+s
		α = 3°	+1	+	+2	+	–	–	+s
		α = 1°	+1	+	+2	+	–	–	+

Table 7. Phase content after 3000 hours steam oxidation at 800°C of austenitic steels: +1 1ˢᵗ, most dominating phase, +2 the 2ⁿᵈ most dominating phase, + presence of a phase, s – trace quantities

Material	Time, h	Geometry	Cr_2O_3	$MnCr_2O_4$	$FeMn(SiO_4)$	Mn_7SiO_{12}	SiO_2	Fe_3O_4
310S	3000	BB	+ 2	+ 1	+	+	+	+ 1
		$\alpha = 3°$	+	+ 2	+	+ 1	+	+ 2
		$\alpha = 1°$	+	+ 2	+	+ 1	+	+ 2
309S	3000	BB	+ 2	+	+	+ 1	+	+
		$\alpha = 3°$	+	+ 2	+	+ 1	+	+ 2
		$\alpha = 1°$	+	+ 2	+	+ 1	+	+ 2
HR3C	3000	BB	+ 1	+ 2	+	–	+	+ 2
		$\alpha = 3°$	+ 2	+ 1	+	–	+	+ 1
		$\alpha = 1°$	+ 2	+ 1	+	–	+	+ 1

Table 8. Phase content after 3000 hours steam oxidation at 800°C of Ni based alloys: +1 1ˢᵗ, most dominating phase, +2 the 2ⁿᵈ most dominating phase, + presence of a phase

Material	Time, h	Geometry	Cr_2O_3	$MnCr_2O_4$	$FeCr_2O_4$	TiO_2	$NiCr_2O_4$	Co_3W_3C
alloy 263	3000	BB	+ 1	+	–	+ 2	–	–
		$\alpha = 3°$	+ 2	+	–	+ 1	–	–
		$\alpha = 1°$	+	+ 2	–	+ 1	–	–
alloy 617	3000	BB	+ 1	–	–	–	+ 2	–
		$\alpha = 3°$	+ 1	–	–	–	+ 2	–
		$\alpha = 1°$	+ 1	–	–	–	+ 2	–
Haynes® 230®	3000	BB	+ 1	+ 2	–	–	–	+
		$\alpha = 3°$	+ 1	+ 2	–	–	–	–
		$\alpha = 1°$	+ 1	+ 2	–	–	–	–
Haynes® 282®	3000	BB	+ 1	+	+	+ 2	–	–
		$\alpha = 3°$	+ 1	+	+	+ 2	–	–
		$\alpha = 1°$	+	+ 2	+ 2	+ 1	–	–

5. Conclusions

The aim of this paper was to evaluate oxide-rich phase formation based on XRD investigations of two solid-solution strengthened alloys; Haynes® 230®, 617 alloy and two (γ') gamma-prime strengthened alloys; 263 and Haynes® 282® and high alloyed steels rich in Cr: 309S, 310S and HR3C that were exposed in steam conditions at high temperatures for 3000 hours. Based on the results achieved here, the following conclusions can be made:

– Both type of materials (Ni based alloys, austenitic steels) developed oxide scales consisting mainly of Cr_2O_3 and $MnCr_2O_4$.

– Austenitic steels at 700 and 800°C developed oxide scale with a high quantity of Fe_3O_4 phase.

– Steels with the addition of Si (309S, 310S) developed Si containing phases: $FeMn(SiO_4)$, Mn_7SiO_{12}, SiO_2.

– Cr doping in TiO_2 increased corrosion degradation by the formation of a higher number of defects and enlargement of mass transport throughout point defects in gamma prime Ni based alloys.

Acknowledgments

References

1. Wright I.G., A. Sabau, R. Dooley. 2008. "Development of strain in oxides grown in steam tubes". *Materials Science Forum* 595−598 : 387−395.

2. *Technology Roadmap: High-efficiency, low-emissions coal-fired power generation*. 2012. Paris: International Energy Agency (IEA).

3. Dudziak T., V. Deodeshmukh, L. Backert, N. Sobczak, M. Witkowska, W. Ratuszek, K. Chruściel, A. Zieliński, J. Sobczak, G. Bruzda. 2017. "Phase investigations under steam oxidation process at 800°C for 1000 h of advanced steels and Ni-based alloys". *Oxidation of Metals* 87 (1−2) : 139−158.

4. Othman N.K., N. Othman, J. Zhang, D.J. Young. 2009. "Effects of water vapour on isothermal oxidation of chromia-forming alloys in Ar/O$_2$ and Ar/H$_2$ atmospheres". *Corrosion Science* 51 (12) : 3039−3049.

5. Pujilaksono B., T. Jonsson, H. Heidari, M. Halvarsson, J.-E. Svensson, L.-G. Johansson. 2011. "Oxidation of binary FeCr alloys (Fe−2.25Cr, Fe−10Cr, Fe−18Cr and Fe−25Cr) in O$_2$ and in O$_2$ + H$_2$O environment at 600°C". *Oxidation of Metals* 75 (3−4) : 183−207.

6. Evans H.E., A.T. Donaldson, T.C. Gilmour. 1999. "Mechanisms of breakaway oxidation and application to a chromia-forming steel". *Oxidation of Metals* 52 (5−6) : 379−402.

7. Bsat S., X. Huang. 2015. "Corrosion behaviour 310 stainless steel in superheated steam". *Oxidation of Metals* 84 (5−6) : 621−631.

8. Saunders S.R.J., M. Monteiro, F. Rizzo. 2008. "The oxidation behaviour of metals and alloys at high temperatures in atmospheres containing water vapour: A review". *Progress in Materials Science* 53 (5) : 775−837.

9. Asteman H., K. Segerdahl, J.E. Svensson, L.G. Johansson. 2001. "The influence of water vapor on the corrosion of chromia-forming steels". *Materials Science Forum* 369−372 : 277−286.

10. Yang Z.G., G.G. Xia, J.W. Stevenson, P. Singh. 2005. *Observations on the oxidation of Mn-modified Ni-base Haynes 230 alloy under SOFC exposure conditions*. U.S. Department of Energy, PNNL-15304.

11. Holcomb G.R., D.E. Alman. 2006. "Effect of manganese additions on the reactive evaporation of chromium in Ni-Cr alloys". *Scripta Materialia* 54 (10) : 1821−1825.

12. Sachitanand R., M. Sattari, J.-E. Svensson, J. Froitzheim. 2013. "Evaluation of the oxidation and Cr evaporation properties of selected FeCr alloys used as SOFC interconnects". *International Journal of Hydrogen Energy* 38 (35) : 15328−15334.

13. Holcomb G.R., D.E. Alman. 2006. *The effect of manganese additions on the reactive evaporation of chromium in Ni-Cr alloys*. Albany Research Center, U.S. Department of Energy, DEO/ARC-05-002.

14. Deodeshmukh V.P. 2013. "Long-term performance of high-temperature foil alloys in water vapor containing environment. Part I: Oxidation behavior". *Oxidation of Metals* 79 (5−6) : 567−578.

15. Pedrazzini S., D.J. Child, G. West, S.S. Doak, M.C. Hardy, M.P. Moody, P.A.J. Bagot. 2016. "Oxidation behaviour of a next generation polycrystalline Mn containing Ni-based superalloy". *Scripta Materialia* 113 : 51−54.

16. Bjørheim T.S., A. Kuwabara, T. Norby. 2013. "Defect chemistry of rutile TiO$_2$ from first principles calculations". *The Journal of Physical Chemistry C* 117 (11) : 5919−5930.

17. Du H.L., P.K. Datta, Z. Klusek, J.S. Burnell-Gray. 2004. "Nanoscale studies of the early stages of oxidation of a TiAl-base alloy". *Oxidation of Metals* 62 (3−4) : 175−193.

18. Kekare S.A., P.B. Aswath. 1997. "Oxidation of TiAl based intermetallics". *Journal of Materials Science* 32 (9) : 2485−2499.

19. Cruchley S., H.E. Evans, M.P. Taylor, M.C. Hardy, S. Stekovic. 2013. "Chromia layer growth on a Ni-based superalloy: Sub-parabolic kinetics and the role of titanium". *Corrosion Science* 75 (October 2013) : 58−66.

20. Chen J.H., P.M. Rogers, J.A. Little. 1997. "Oxidation behavior of several chromia-forming commercial nickel-base superalloys". *Oxidation of Metals* 47 (5−6) : 381−410.

21. Kim D., C. Jang, W.S. Ryu. 2009. "Oxidation characteristics and oxide layer evolution of alloy 617 and Haynes 230 at 900°C and 1100°C". *Oxidation of Metals* 71 (5−6) : 271−293.

22. Taylor M.P., H.E. Evans, S. Stekovic, M.C. Hardy. 2012. "The oxidation characteristics of the Ni-based superalloy, RR1000, at temperatures 700−900°C". *Materials at High Temperatures* 29 : 145−150.

23. Fry A., S. Osgerby, M. Wright. 2002. *Oxidation of alloys in steam environments – A Review*. United Kingdom: NPL Materials Centre.

24. Bauer R., M. Baccalaro, L.P.H. Jeurgens, M. Pohl, E.J. Mittemeijer. 2008. "Oxidation behavior of Fe–25Cr–20Ni–2.8Si during isothermal oxidation at 1,286 K; Lifetime Prediction". *Oxidation of Metals* 69 (3−4) : 265−285.

25. Evans H.E., D.A. Hilton, R.A. Holm, S.J. Webster. 1983. "Influence of silicon additions on the oxidation resistance of a stainless steel". *Oxidation of Metals* 19 (1−2) : 1−18.

26. Henry S., A. Galerie, L. Antoni. 2001. "Abnormal oxidation of stabilized ferritic stainless steels in water vapor". *Materials Science Forum* 369−372 : 353–360.

27. Ennis P., W. Quadakkers. 2007. "Implications of steam oxidation for the service life of high-strength martensitic steel components in high-temperature plant". *International Journal of Pressure Vessels and Piping* 84 (1−2) : 82−87.

28. Jonsson T., S. Karlsson, H. Hooshyar, M. Sattari, J. Liske, J.-E. Svensson, L.-G. Johansson. 2016. "Oxidation after breakdown of the chromium-rich scale on stainless steels at high temperature: Internal oxidation". *Oxidation of Metals* 85 (5−6) : 509−536.

29. Hansson A.N., K. Pantleon, F.B. Grumsen, M.A.J. Somers. 2010. "Microstructure evolution during steam oxidation of a Nb stabilized austenitic stainless steel". *Oxidation of Metals* 73 (1−2) : 289−309.

30. Essuman E., G.H. Meier, J. Żurek, M. Hänsel, L. Singheiser, W.J. Quadakkers. 2007. "Enhanced internal oxidation as trigger for breakaway oxidation of Fe–Cr alloys in gases containing water vapor". *Scripta Materialia* 57 (9) : 845−848.